



OPEN

## Copper(II)- $\beta$ -cyclodextrin immobilized on graphitic carbon nitride nanosheets as a highly effective catalyst for tandem oxidative amidation of benzylic alcohols

Hossein Ghafari<sup>✉</sup>, Afsaneh Rashidizadeh, Mostafa Ghafari Gorab & Ghazaleh Jafari

In this study, an efficient catalyst based on graphitic carbon nitride nanosheets (CN) and copper(II) supported  $\beta$ -cyclodextrin ( $\beta$ -CD/Cu(II)) was synthesized and used for tandem oxidative amidation of benzylic alcohols. In this regard, CN was functionalized by  $\beta$ -CD/Cu(II) via 1,3-dibromopropane linker (CN-Pr- $\beta$ -CD/Cu(II)). The prepared catalyst was characterized using FT-IR, XRD, FE-SEM, EDS, TGA, ICP-OES, BET, and TEM analyses. CN-Pr- $\beta$ -CD/Cu(II) was subsequently applied in a direct oxidative amidation reaction and it was observed that different benzylic alcohols were converted to desired amides with good to excellent efficiency. This reaction was performed in the presence of amine hydrochloride salts, tert-butyl hydroperoxide (TBHP), and  $\text{Ca}_2\text{CO}_3$  in acetonitrile ( $\text{CH}_3\text{CN}$ ) under nitrogen atmosphere. CN-Pr- $\beta$ -CD/Cu(II) can be recycled and reused five times without significant reduction in reaction efficiency.

Amides are one of the most important functional groups in various industrial and scientific research fields such as polymers, drugs, chemical raw materials, biomolecules, and natural products<sup>1–4</sup>. Numerous methods have been reported for the synthesis of these valuable materials<sup>5,6</sup>. Traditionally, the vast majority of amides were prepared through interaction of amines with active or inactive carboxylic acid derivations<sup>7,8</sup>. In addition, reactions such as Schmidt<sup>9</sup>, Ugi<sup>10</sup>, Staudinger<sup>11</sup>, and Ritter<sup>12</sup>, were used to synthesize amides. Risks or negative effects of these methodologies have led to the creation of lower risk protocols. Recently, various modified procedures like oxidative amidations reactions<sup>13</sup>, primary amides transamination via amines<sup>14</sup>, alkynes hydroamination<sup>15</sup>, and amines acylation have been described<sup>16</sup>. Among established synthetic methods, one of the greenest procedures is amide formation via tandem oxidative amidation of benzylic alcohols by transition metal catalysts. Various metals such as “Ru”<sup>17</sup>, “Rh”<sup>18</sup>, “Zn”<sup>19</sup>, “Fe”<sup>20</sup>, “Au”<sup>21</sup>, “Ir”<sup>22</sup>, and “Cu”<sup>23</sup> can be used in this reaction as catalysts. Among the reported metals, copper due to the natural abundance, high activity, and low price was considered as an attractive option to catalyze these reactions<sup>24</sup>. However, one of the main problems of these metals as catalysts is the difficulty of their separation from the reaction medium. To overcome this problem, these metals are usually coordinated on a solid surface via appropriate ligands. In this regard, various materials like graphene oxide, Nitrogen-doped (N-doped) graphene, hexagonal boron nitride, metal chalcogenide, and graphitic carbon nitride ( $\text{g-C}_3\text{N}_4$ ) can be used<sup>25</sup>.  $\text{g-C}_3\text{N}_4$  as a metal-free polymeric structure with two-dimensional layered morphology, has attracted special attention due to the features such as chemical and thermal stability, wide surface area, and biocompatibility<sup>26</sup>. CN, as one of the most important forms of  $\text{g-C}_3\text{N}_4$  has many applications in fields of dyes photodegradation<sup>27</sup>, solar energy<sup>28</sup>, supercapacitors<sup>29</sup>, water splitting<sup>30</sup>, sensors<sup>31</sup>, hydrogen evolution<sup>32</sup>, and catalysts<sup>33</sup>. Ligands also play a very important role in the coordination of metal on a solid support, and in this regard,  $\beta$ -Cyclodextrin ( $\beta$ -CD) has been considered.  $\beta$ -CD is cyclic oligosaccharides, made up from seven D-glucopyranose parts.  $\beta$ -CD conical cylinder framework has an inner lipophilic space as well as an outer hydrophilic one<sup>34</sup>. During recent years,  $\beta$ -CD special features and ability of creation complex have

Catalysts and Organic Synthesis Research Laboratory, Department of Chemistry, Iran University of Science and Technology, 16846-13114 Tehran, Iran. ✉email: ghafari@iust.ac.ir

attracted major attention in the areas of food<sup>35</sup>, medicine<sup>36</sup>, textile<sup>37</sup>, cosmetology<sup>38</sup>, enantiomeric separation<sup>39</sup>, environmental remediation<sup>40</sup>, chemical sensing<sup>41</sup>, and catalysis<sup>42</sup>. Combining CN with various metal supported  $\beta$ -CD structures for catalytic and photocatalytic reactions have become an attractive strategy in improving the performance of reactions<sup>43,44</sup>. For example, in the study performed by Zuo and et al. in 2020, Au nanoparticles were coordinated on  $\beta$ -CD modified g-C<sub>3</sub>N<sub>4</sub>. This nanocomposite was used in the photocatalytic production of hydrogen peroxide<sup>43</sup>. Herein, CN was functionalized by  $\beta$ -CD/Cu(II) and this modification was performed by 1,3-dibromopropane as a linker. CN-Pr- $\beta$ -CD/Cu(II) was used as a catalyst in tandem oxidative amidation of benzylic alcohols and various derivatives were synthesized with good to excellent efficiencies.

## Experimental

**Reagents and instruments.** In this study, all used materials were purchased from reputable international companies, including Flucka (Switzerland) and Merck (United States). The reaction conditions were controlled by Thin Layer Chromatography (TLC) by utilizing a 0.2 mm F254 Merck silica gel coated on aluminum plates (United States). Also, the accuracy of forming the products was investigated using the melting point with the electrothermal 9100 device (United Kingdom). 800 IR 100 device from Shimadzu company was used for the record Fourier transform (FT)-IR spectra to identify catalysts and reaction products (Japan). This analysis was performed in the range of 400–4000 cm<sup>-1</sup>. The X-ray diffraction (XRD) analysis was used to identify the crystal structure of the catalyst components and PANalytical X-PERT-PRO MPD apparatus was used for this purpose (Netherlands). This analysis was evaluated in the range of 2 $\theta$ , 0.5° to 10° and 10° to 80°. Energy Dispersive X-ray Spectroscopy (EDS) was performed by ZEISS-Sigma VP (Germany) in order to examine the elements of the catalyst. Field emission scanning electron microscopy (FE-SEM) by MIRA3 TESCAN-XMU instrument (Czechia), Thermogravimetric analysis (TGA) by STA504 device (United States) and inductively coupled plasma optical emission spectroscopy (ICP-OES) by VISTA-PRO (United States) were used to evaluate the morphology, thermal stability and recyclability of the catalyst, respectively. N<sub>2</sub> adsorption/desorption isotherms was used to investigate the surface area of the synthesized catalyst. For this purpose, 2020 ASAP™ apparatus made by American company micromeritics was used. Transmission electron microscopy (TEM) imaging was performed using the EM10C-100 kV device made by the German company ZEISS to investigate the dispersion of metal particles in the catalyst structure.

**Preparation of Bulk g-C<sub>3</sub>N<sub>4</sub>.** First 5 g of white melamine powder heated for 4 h at 550 °C by laboratory furnace under static air. This process was done with a temperature ramp of 2.5 °C min<sup>-1</sup>. Finally, the resulting yellow solid was grinded to powder particles<sup>45</sup>.

**Preparation of CN.** The procedure utilized to prepare the nanosheet form of the g-C<sub>3</sub>N<sub>4</sub> was introduced by Li and et al.<sup>46</sup>. First, 1 g of the synthesized g-C<sub>3</sub>N<sub>4</sub> was dispersed in a mixture containing 20 ml of nitric acid (65 wt%) and 20 ml of sulfuric acid (98 wt%) for 2 h at ambient temperature. Then, 1 L of deionized water was added to dilute the mixture. The precipitate was collected and washed several times with deionized H<sub>2</sub>O, and finally dried in an oven at 60 °C. In the next step, 1 mg of g-C<sub>3</sub>N<sub>4</sub> was dispersed in 100 ml of H<sub>2</sub>O/isopropanol (1:1) for 6 h by an ultrasonic bath. Eventually, a centrifuge with speed of 5000 RPM was used to separate the synthesized CN.

**Preparation of CN-Pr-Br.** 1 g of the synthesized CN was added to 25 ml of dry toluene and the mixture was sonicated for 1 h. Then, 1 mmol of sodium iodide and 2.02 ml of 1,3-dibromopropane were added to the dispersed mixture and the reaction suspension was refluxed under nitrogen atmosphere for 2 days. The functionalized CN was separated by centrifugation and dried at ambient temperature.

**Preparation of  $\beta$ -CD/Cu(II).** The copper and  $\beta$ -CD complex was constructed using a method reported by Kaboudin and et al.<sup>47</sup>. Initially, 1 mmol of  $\beta$ -CD was added to 250 ml beaker including 50 ml of 1 M sodium hydroxide solution, and the mixture was stirred until a clear solution was formed. Afterward, 75 ml solution contain 0.04 M of CuSO<sub>4</sub>(H<sub>2</sub>O)<sub>5</sub> salt was added to the clear solution prepared in the previous step. The dark blue solution obtained at this stage was stirred at 25 °C for 6 h. After this time, the mixture was passed through filter paper to separate the excess copper as copper (II) hydroxide. Finally, 400 ml of ethanol was added to the remaining solution to form a pale blue suspension. The precipitate was separated by the Buchner funnel and after washing with ethanol, dried at 60 °C.

**Preparation of CN-Pr- $\beta$ -CD/Cu(II).** 0.1 g of the functionalized CN and 20 ml of dry toluene were added to a 50 ml flask and sonicated for 30 min. Then, 0.1 g of  $\beta$ -CD/Cu(II) complex, 0.1 mmol of sodium iodide and 0.1 mmol of potassium carbonate were added to the reaction vessel and refluxed under N<sub>2</sub> for 2 days. Eventually, the precipitate was collected by centrifugation, washed several times with water and ethanol, and dried in a 60 °C oven.

**General Procedure for the Tandem oxidative amidation of benzylic alcohols catalyzed by CN-Pr- $\beta$ -CD/Cu(II).** To a 10 ml round bottom flask, 1.5 mmol of benzyl alcohol, 1 mmol of hydrochloride salt of amine, 1/1 equivalents of calcium carbonate, 3 equivalents of TBHP, 15 mg of CN-Pr- $\beta$ -CD/Cu(II), and 3 ml of CH<sub>3</sub>CN were added. The mentioned materials were then refluxed under N<sub>2</sub> for 3 h at 80 °C. After the completion of the reaction was confirmed using TLC, the catalyst was separated by filter paper and washed

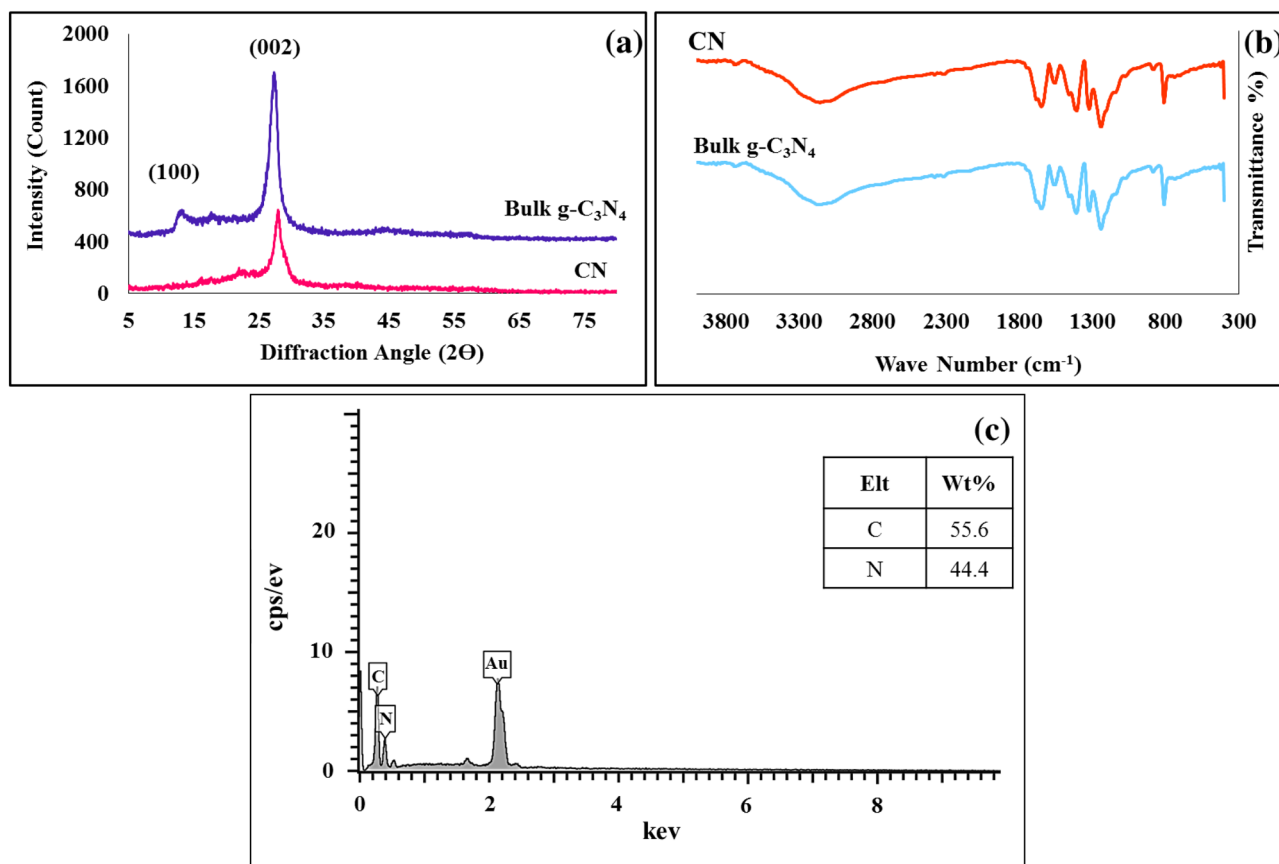


**Figure 1.** (a) XRD patterns and (b) FT-IR spectra of bulk  $g\text{-C}_3\text{N}_4$  and CN. (c) EDS spectrum of the CN.

through ethanol for subsequent use. Eventually, the  $\text{CH}_3\text{CN}$  was evaporated by a rotary, and the product was extracted ( $\text{H}_2\text{O}$ /ethyl acetate) and recrystallized (by ethanol) for further purification.

## Results and discussion

**Catalyst characterization.** In this study, CN-Pr- $\beta$ -CD/Cu(II) was prepared by a facile procedure. Initially, CN with two-dimensional morphology were prepared via exfoliation in liquid phase and then the layers were separated by ultrasonic treatment. XRD, FT-IR and EDS analysis were used to confirm the correct formation of CN and they were demonstrated in Fig. 1. According to information obtained from XRD analysis, bulk  $g\text{-C}_3\text{N}_4$  has been converted to nanosheets form of the  $g\text{-C}_3\text{N}_4$ . The XRD spectrum of bulk  $g\text{-C}_3\text{N}_4$  has two main peaks in  $2\theta = 27.4^\circ$  and  $13.1^\circ$  which is related to the interaction between conjugated aromatic part of the system and tri-s-triazine units of the structure (Fig. 1a). After exfoliation, the peak intensity of the (002) decreases and its  $2\theta$  position shifts from  $27.4^\circ$  to  $27.8^\circ$ , which may be related to the distance between the  $g\text{-C}_3\text{N}_4$  layers. Also during this process, another  $g\text{-C}_3\text{N}_4$  peak in  $2\theta = 13.1^\circ$  was removed<sup>26</sup>. In addition, the value of d-spacings for the peaks observed in  $27.4^\circ$  and  $13.1^\circ$  for bulk  $g\text{-C}_3\text{N}_4$  is 0.325 nm and 0.675 nm, respectively<sup>48</sup>. After the exfoliation process and CN synthesis, the value of d-spacings for the peak in  $2\theta = 27.8^\circ$  is equal to 0.321 nm. The slight decrease observed in d-spacings during peak displacement from  $27.4^\circ$  to  $27.8^\circ$  is due to the flattening of the undulated layers in  $g\text{-C}_3\text{N}_4$ . In other words, the heat and oxidation applied to convert bulk  $g\text{-C}_3\text{N}_4$  to nanosheets, compress the CN monolayers together and shorten the interplane distance of the CN sample<sup>49</sup>.

The FT-IR spectra of bulk  $g\text{-C}_3\text{N}_4$  and CN are similar to each other. According to Fig. 1b, the peak observed in the range of  $3000\text{--}3500\text{ cm}^{-1}$  was related to N-H present on the  $g\text{-C}_3\text{N}_4$ . Also, the observed peaks in the range of  $1614\text{ cm}^{-1}$  and  $1550\text{ cm}^{-1}$  corresponded to the stretching vibration of C=N. C-N stretching peaks were located in  $1406\text{ cm}^{-1}$ ,  $1319\text{ cm}^{-1}$ , and  $1234\text{ cm}^{-1}$ . Also sharp peak at  $808\text{ cm}^{-1}$  was related to the breathing vibration of the tri-s-triazine components. EDS confirmed the presence of carbon and nitrogen in the  $g\text{-C}_3\text{N}_4$  structure (Fig. 1c). Subsequently, 1,3-dibromopropane was used to modify the CN and the linker binding process was examined by FT-IR and EDS analyzes. As can be seen in Fig. 2a, the FT-IR spectrums of CN-Pr-Br and linker-free CN were identical. On the other hand and based on Fig. 2b, EDS analysis confirmed the presence of the Br atoms. Finally, to increase the stability of  $\beta$ -CD/Cu(II) and also to promote the catalytic properties and dispersion of CN in water, CN-Pr- $\beta$ -CD/Cu(II) were synthesised. As presented in Fig. 3a, the main peaks for the  $\beta$ -CD structure, including the sharp peak at  $2920\text{ cm}^{-1}$  and the wide peak at  $3369\text{ cm}^{-1}$ , can be related to the stretching vibrations of the C-H and OH bonds, respectively. In addition, glucose peaks, including C-C, C-O, and C-O-C, are found in the areas of  $1027\text{ cm}^{-1}$ ,  $1155\text{ cm}^{-1}$ ,  $1340\text{ cm}^{-1}$ ,  $1417\text{ cm}^{-1}$ ,  $1647\text{ cm}^{-1}$ . FT-IR spectrum of copper (II) supported  $\beta$ -CD, confirm complex formation of the  $\beta$ -CD with copper (II). According to this spectrum, the

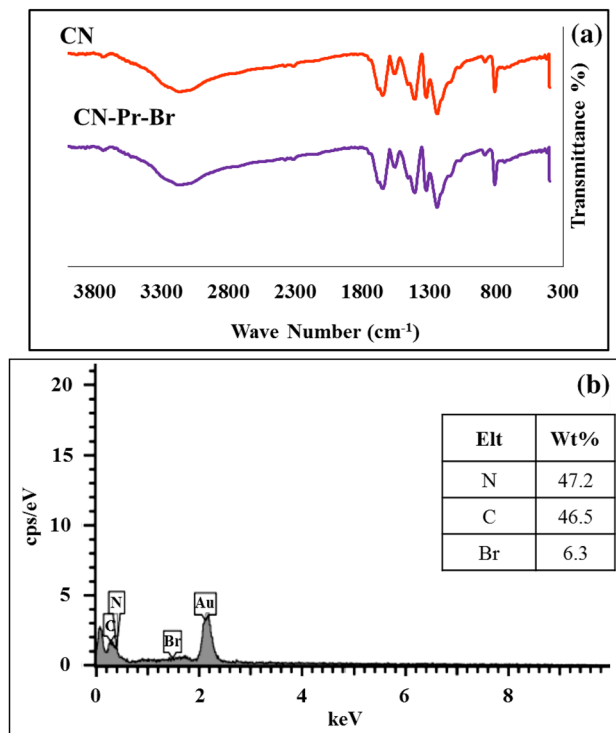


**Figure 2.** (a) FT-IR spectra of CN and CN-Pr-Br. (b) EDS analysis of CN-Pr-Br.

absorption frequencies in the  $\beta$ -CD structure were shifted to lower frequencies. This shifts to lower frequencies were confirmed the  $\beta$ -CD complexation with copper. Eventually, by comparing the CN-Pr- $\beta$ -CD/Cu(II) spectrum with the spectra of raw materials in previous stages, it can be concluded that the presence of absorption bands in  $2948\text{ cm}^{-1}$  are related to the CH stretching vibrations in the  $\beta$ -CD molecule and the 1,3-dibromopropane linker. Moreover, the absorption band at  $1110\text{ cm}^{-1}$  was confirmed the formation of a CO bond in the final catalyst. The main adsorption bands relevant to the structure of CN and  $\beta$ -CD are exist in final structure of the catalyst.

In the next step, the elements in the structure of the  $\beta$ -CD/Cu(II) and CN-Pr- $\beta$ -CD/Cu(II) were examined by EDS analysis. As can be seen in Fig. 3b,c,  $\beta$ -CD/Cu(II) contains carbon, oxygen, copper and on the other hand, CN-Pr- $\beta$ -CD/Cu(II) includes carbon, nitrogen, bromine, oxygen and copper. ICP-OES was also utilized to determine the amount of copper in the structure of the CN-Pr- $\beta$ -CD/Cu(II) and the presence of 12.7% copper in the catalyst structure was confirmed. FE-SEM and TEM imaging were performed to evaluate the structure and morphology of the catalyst. The FE-SEM images of CN and CN-Pr- $\beta$ -CD/Cu(II) are shown in Fig. 4a and Fig. 4b,c respectively. Accordingly, CN plates and the functionalization process were well observed. On the other hand, as seen in the TEM image of CN-Pr- $\beta$ -CD/Cu(II) in Fig. 4d,e, acceptable dispersion for metal particles were observed in the catalyst structure.

The XRD patterns of CN,  $\beta$ -CD, and CN-Pr- $\beta$ -CD/Cu(II) were indicated in Fig. 5a. As shown in spectrum of the CN-Pr- $\beta$ -CD/Cu(II), diffractions peaks related to the structure of  $\beta$ -CD were observed in the XRD diagram of the catalyst which confirm the functionalization of the CN. Furthermore, the diffractions peak at  $2\theta$  about  $60.0^\circ$  is related to the copper in the structure of the CN-Pr- $\beta$ -CD/Cu(II) catalyst. TGA used to investigate the thermal stability of the synthesized samples. The TGA diagram for CN and the final catalyst was shown in Fig. 5b,c respectively. According to the Fig. 5b, the main mass loss of the CN begin at  $600^\circ\text{C}$ . Figure 5c shows the CN-Pr- $\beta$ -CD/Cu(II) TGA curve. In this diagram, three main mass reduction steps were observed, 3% mass reduction observed in the range of  $201\text{--}106^\circ\text{C}$ , which can be related to the evaporation of water and the exit of solvents trapped in the structure. The 16% mass drop in the range of  $401\text{--}203^\circ\text{C}$  was related to the breakdown of the linker and part of the  $\beta$ -CD. Finally, the mass drop at temperatures above  $400^\circ\text{C}$  was due to the complete loss of  $\beta$ -CD and CN. Finally, it can be concluded that the functionalization process occurred well and during this process, the thermal stability of  $\beta$ -CD/Cu(II) increased. BET analysis was also performed to evaluate the surface area of the synthesized catalyst via nitrogen adsorption-desorption equilibrium (Fig. 5d). According to the obtained results, the BET surface area of the synthesized catalyst was  $90.2127\text{ m}^2/\text{g}$ . The catalytic capacitance of CN-Pr- $\beta$ -CD/Cu(II) was reconnoitered for the preparation of amide derivatives via oxidation of benzylic alcohols with the amine hydrochloride salts. An overview of this process can be found in Fig. 6. To perform the reaction, the effective parameters in the reaction were first optimized to achieve the highest efficiency. As shown in Table 1, the effect of different factors on the reaction including catalyst, oxidizing agent, base, temperature and solvent was investigated.

The model reaction performed by 20 mg CN-Pr- $\beta$ -CD/Cu(II) catalyst and 3 equivalents of TBHP in the presence of calcium carbonate. Based on the observed results, the presence of both base and oxidizing agents

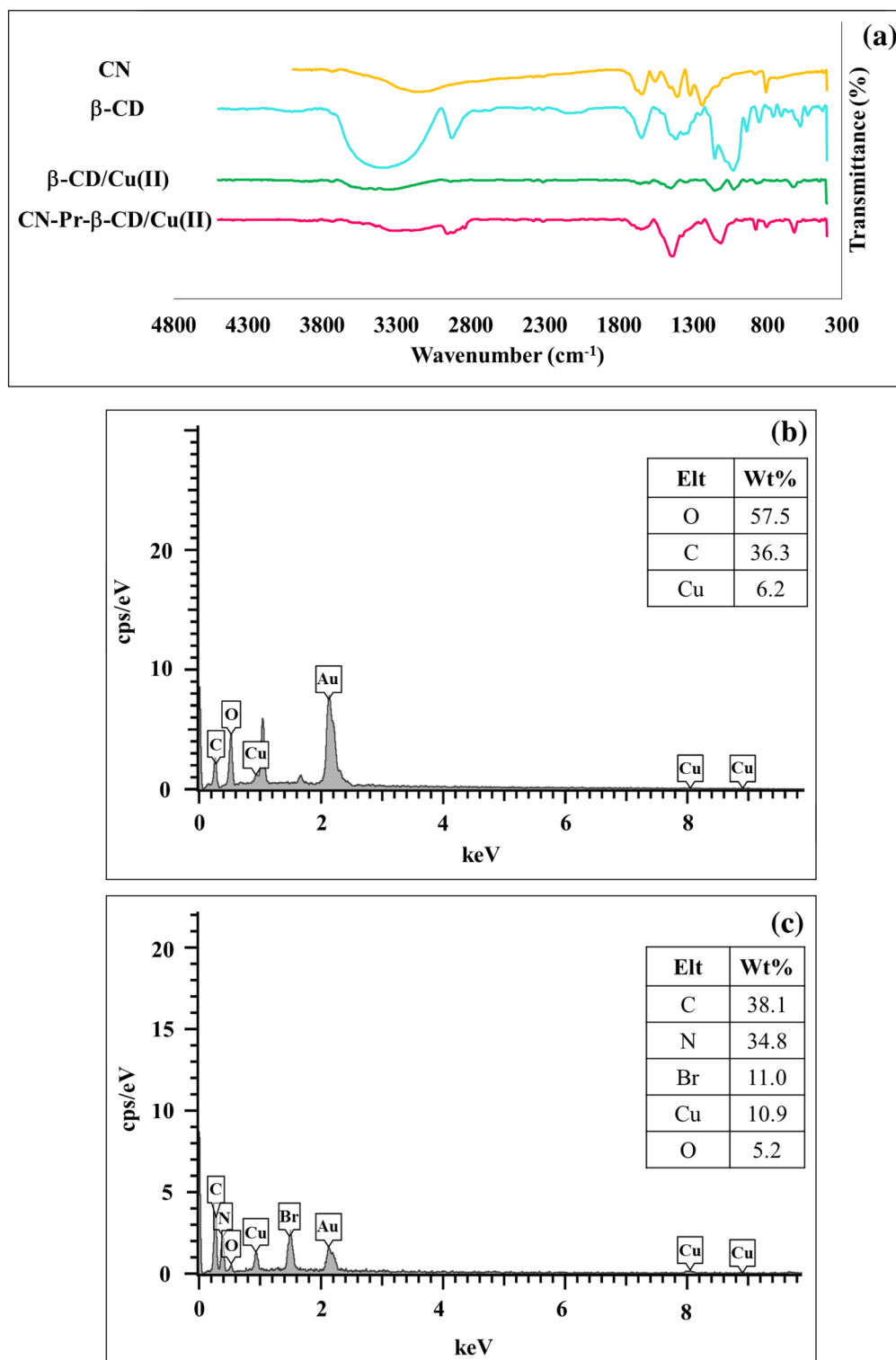


**Figure 3.** (a) FT-IR spectra of CN,  $\beta$ -CD,  $\beta$ -CD/Cu(II), CN-Pr- $\beta$ -CD/Cu(II), (b) EDS analysis of  $\beta$ -CD/Cu(II), and (c) EDS analysis of CN-Pr- $\beta$ -CD/Cu(II).

is necessary for the reaction to take place (Rows 1–3, Table 1). This reaction was accomplished at 80 °C in  $\text{CH}_3\text{CN}$  solvent under  $\text{N}_2$  atmosphere (Row 4, Table 1). Under these conditions, *N*-benzylbenzamide was obtained with 80% efficiency. Then, the effect of various factors including the amount of oxidizing agent, the type of oxidizing agent, the quantity of catalyst, the reaction temperature, the type of base, and the reaction solvent were investigated. Reducing the amount of TBHP to 3 equivalents, increases the production efficiency of the target product (90%) (Row 6, Table 1). In the next step, the amount of catalyst used in the reaction was



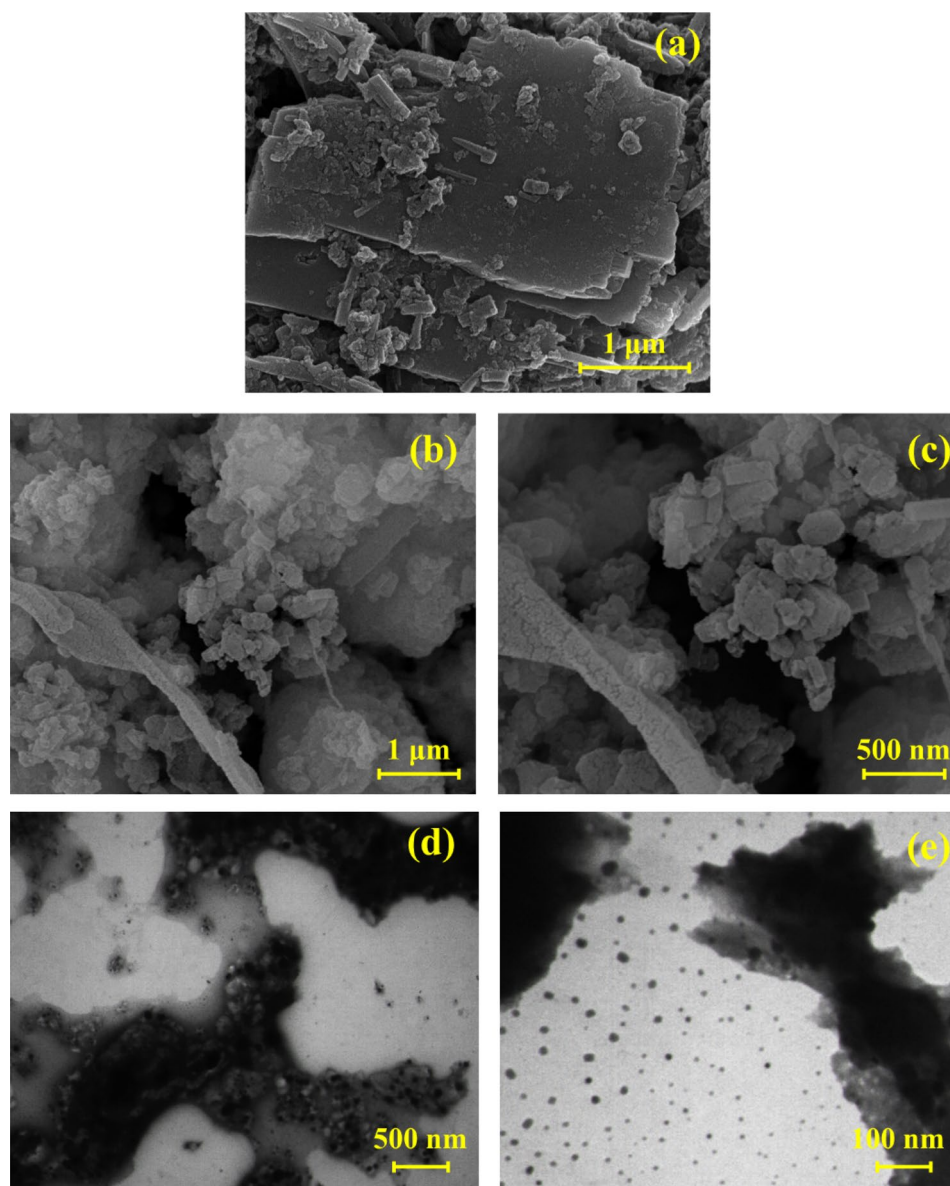


**Figure 4.** FE-SEM images of (a) CN, (b,c) CN-Pr-β-CD/Cu(II) and, (d,e) TEM images of CN-Pr-β-CD/Cu(II).

investigated. As shown in Row 8 of Table 1, 15 mg of CN-Pr-β-CD/Cu(II) catalyst had the best effect at reaction efficiency (95%). Hydrogen peroxide ( $H_2O_2$ ) and oxygen ( $O_2$ ) were used as green oxidizing agents in this reaction (rows 10–11, Table 1). The best yield of the desired amide product was obtained by TBHP under nitrogen atmosphere. In the next step, different temperatures in the range of 60 to 100 were examined (rows 8, 12 and 13, Table 1) and it was observed that increasing the reaction temperature to 100° C reduces the reaction efficiency to 86% (Row 12, Table 1). Decreased in the reaction efficiencies may be related to the oxidation of benzyl alcohol to the related benzoic acid as a by-product that occurred at higher temperatures (benzoic acid by-product formation was confirmed by TLC). Further studies in this area have shown that the best temperature for the reaction was 80° C. Various bases including  $Na_2CO_3$ ,  $K_2CO_3$  and  $CaCO_3$  were used to optimize the reaction conditions (rows 8, 14 and 15, Table 1). Among them, calcium carbonate minimized the adverse oxidation reaction of amine via slow deprotonation of the amine hydrochloride salt. As a result, the yield of the target product was increased. Eventually, the model reaction was done in  $CH_3CN$ , toluene, dimethylformamide (DMF) and dimethyl sulfoxide (DMSO) solvents (rows 8, 16, 17 and 18, Table 1) and the best yield for *N*-benzylbenzamide was obtained in  $CH_3CN$  solvent.

To demonstrate the potential and importance of using the CN-Pr-β-CD/Cu(II) catalyst in the tandem oxidative amidation of benzylic alcohols, the model reaction was performed under optimal condition with the presence of other catalysts such as copper sulfate salt, CN, β-CD, CN/Cu(II) and copper (II) supported β-CD (Table 2). Based on the obtained results in the mentioned table, the CN-Pr-β-CD/Cu(II) catalyst had the highest efficiency in the amide synthesis reaction. The presence of copper is an essential factor in promoting this reaction.

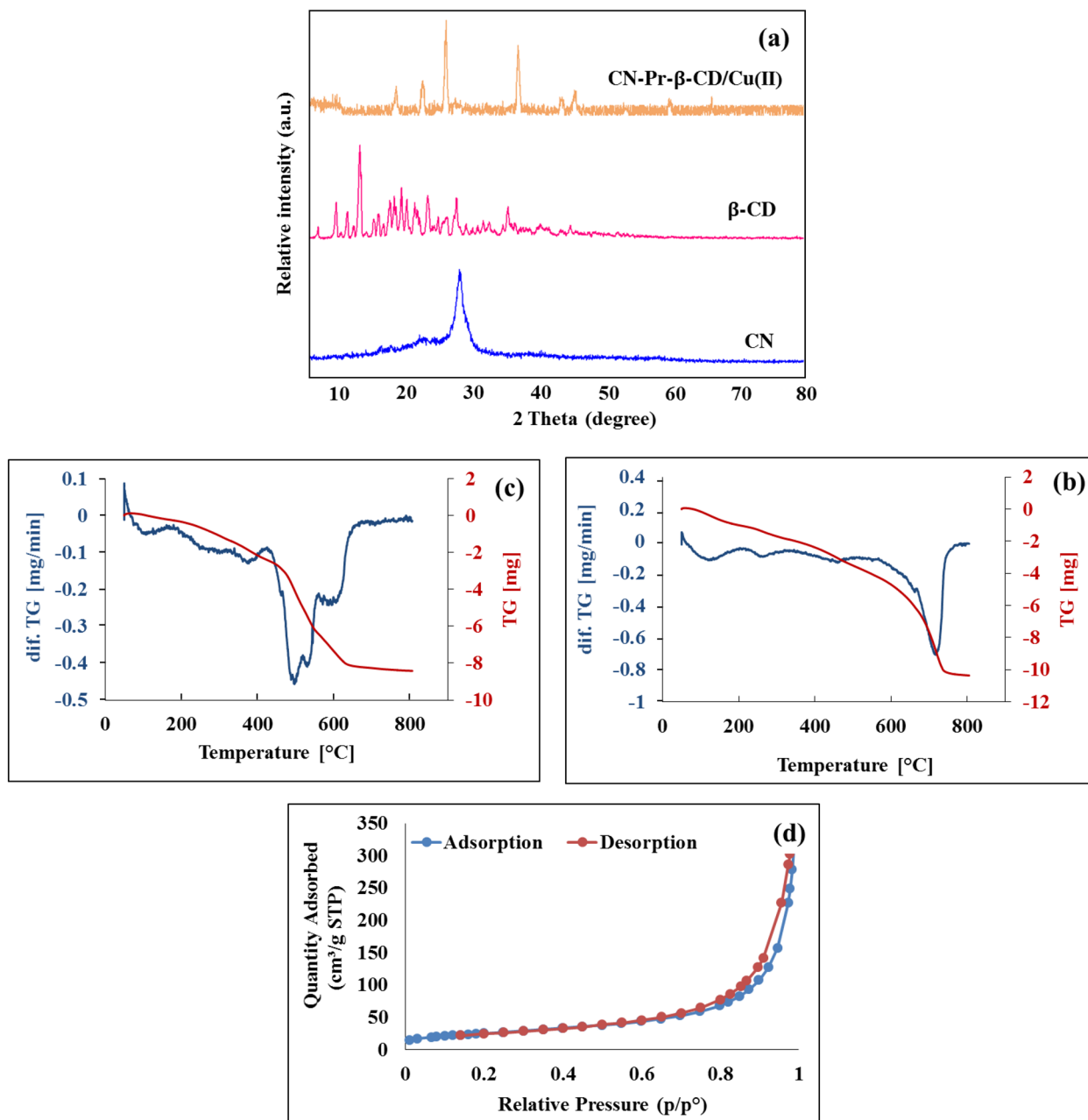


**Figure 5.** (a) XRD patterns of CN, β-CD, CN-Pr-β-CD/Cu(II), (b) TGA patterns of CN, (c) TGA patterns of CN-Pr-β-CD/Cu(II) and, (d) N<sub>2</sub> adsorption–desorption isotherms of CN-Pr-β-CD/Cu(II).

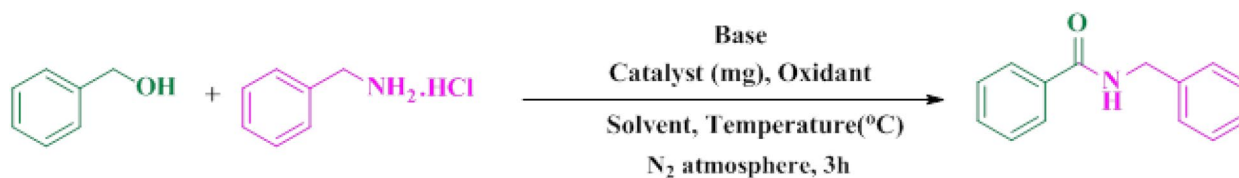


**Figure 6.** Model reaction to optimize the tandem oxidative amidation of benzylic alcohols by CN-Pr-β-CD/Cu(II) catalysts.

After determining the optimal conditions, various amides were synthesized by different benzylic alcohols and amine salts and the results are demonstrated in Table 3. Based on the information shown in Table 3, the oxidative amidation of benzylic alcohols with different aliphatic and aromatic amine hydrochloride salts (types 1, 2, and 3) and different type of benzylic alcohols including electron donor and withdrawing groups has been studied. In all cases the desired amide was obtained with the appropriate yield.

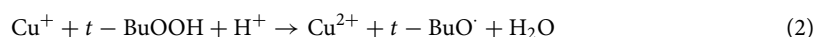
Entry	Solvent	Oxidant	Amount of oxidant (equivalent)	Base	Amount of catalyst (mg)	Temperature (°C)	Yield (%) <sup>a</sup>
1	CH <sub>3</sub> CN	–	–	–	20	80	–
2	CH <sub>3</sub> CN	TBHP	4	–	20	80	–
3	CH <sub>3</sub> CN	–	–	CaCO <sub>3</sub>	20	80	–
4	CH <sub>3</sub> CN	TBHP	4	CaCO <sub>3</sub>	20	80	80
5	CH <sub>3</sub> CN	TBHP	4	CaCO <sub>3</sub>	–	80	–
6	CH <sub>3</sub> CN	TBHP	3	CaCO <sub>3</sub>	20	80	90
7	CH <sub>3</sub> CN	TBHP	3	CaCO <sub>3</sub>	25	80	83
8	CH <sub>3</sub> CN	TBHP	3	CaCO <sub>3</sub>	15	80	95
9	CH <sub>3</sub> CN	TBHP	3	CaCO <sub>3</sub>	10	80	80
10	CH <sub>3</sub> CN	H <sub>2</sub> O <sub>2</sub>	3	CaCO <sub>3</sub>	15	80	30
11	CH <sub>3</sub> CN	O <sub>2</sub>	–	CaCO <sub>3</sub>	15	80	25
12	CH <sub>3</sub> CN	TBHP	3	CaCO <sub>3</sub>	15	100	86
13	CH <sub>3</sub> CN	TBHP	3	CaCO <sub>3</sub>	15	60	80
14	CH <sub>3</sub> CN	TBHP	3	Na <sub>2</sub> CO <sub>3</sub>	15	80	Trace
15	CH <sub>3</sub> CN	TBHP	3	K <sub>2</sub> CO <sub>3</sub>	15	80	–
16	Toluene	TBHP	3	CaCO <sub>3</sub>	15	80	20
17	DMF	TBHP	3	CaCO <sub>3</sub>	15	80	40
18	DMSO	TBHP	3	CaCO <sub>3</sub>	15	80	55

**Table 1.** Optimization of the reaction condition for the one-pot direct oxidative amidation. Reaction condition: benzylamine hydrochloride (1.0 mmol), benzyl alcohol (1.5 mmol), catalyst (CN-Pr-β-CD/Cu(II)), solvent (3 mL), Base (1.1 equiv), oxidant (70 wt % in H<sub>2</sub>O, 3 equiv), under N<sub>2</sub> atmosphere. <sup>a</sup>Isolated yield.

Entry	Catalyst	Yield (%) <sup>a</sup>
1	CN	–
2	CuSO <sub>4</sub> ·5H <sub>2</sub> O	30
3	β-CD	–
4	β-CD/Cu(II)	45
5	CN/Cu(II)	75
6	CN-Pr-β-CD/Cu(II)	95

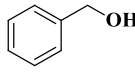
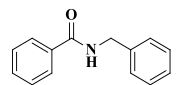
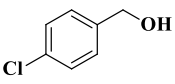
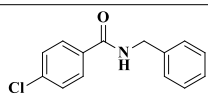
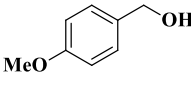
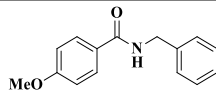
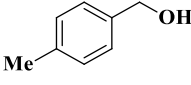
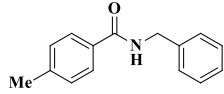
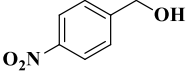
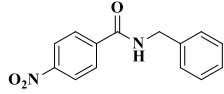
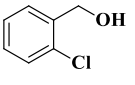
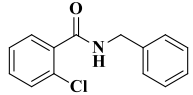
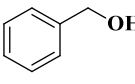
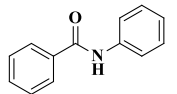
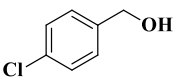
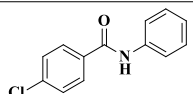
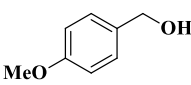
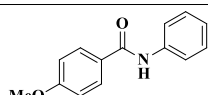
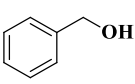
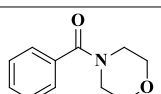
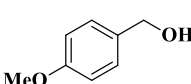
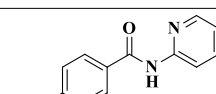
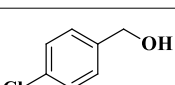
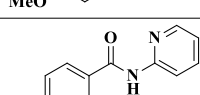
**Table 2.** Comparison of the catalytic performance of CN-Pr-β-CD/Cu(II) with other catalysts in synthesis of amide through the oxidative amidation of benzylic alcohols. Reaction condition: benzylamine hydrochloride (1.0 mmol), benzyl alcohol (1.5 mmol), Catalyst (15 mg), CH<sub>3</sub>CN (3 mL), CaCO<sub>3</sub> (1.1 equiv), TBHP (70 wt % in H<sub>2</sub>O, 3 equiv). <sup>a</sup>Isolated yield.

The outline of the possible mechanism for tandem oxidative amidation of benzylic alcohols was indicated in Fig. 7. TBHP is an excellent source of oxygen and can be used for oxidation reactions after activation by a suitable transition metal complex<sup>66</sup>. In this regard, benzyl alcohol in the presence of CN-Pr-β-CD/Cu(II) and TBHP was oxidized to aldehyde through a radical mechanism and tert-butanol was released. In addition, tert-butylperoxy and tert-butoxy radicals were also produced through Eqs. (1) and (2), respectively<sup>20,67</sup>. In the next step, calcium carbonate as the base separates the proton from the amine hydrochloride salt, and the resulting free amine reacts with the aldehyde and eventually producing the hemiaminal intermediate (III)<sup>20,68</sup>. Reduction of copper (II) ions in the CN-Pr-β-CD/Cu(II) catalyst leads to the production of tert-butyl peroxy radical. Subsequently, the hemiaminal was converted to intermediate (IV) in the presence of the activated tert-butyl peroxy radical. Finally, intermediate (IV) by the CN-Pr-β-CD/Cu(II)-TBHP catalytic system produces the desired amide through a radical mechanism by removing the tert-butanol. Then, to ensure the radical process of the reaction mechanism, 2,6-Di-tert-butyl-4-methylphenol (BHT) was used as a radical scavenger in the model reaction and no product was observed during the reaction. From this, it can be concluded that the oxidation reaction of benzyl alcohols has proceeded in a radical way.



The ability to recycle and reuse the catalyst is one of the most important aspects of catalyst design. In this regard, the CN-Pr-β-CD/Cu(II) catalyst was separated from the other components of the reaction by filter paper



Entry	Alcohol	Amine salt	Product	Yield (%) <sup>a</sup>	Mp. (°C) (Ref.)
1		a		95	108–110 <sup>50</sup>
2		a		90	162–164 <sup>51</sup>
3		a		95	101–103 <sup>52</sup>
4		a		93	132–134 <sup>53</sup>
5		a		75	139–142 <sup>54</sup>
6		a		65	95–97 <sup>55</sup>
7		b		90	160–162 <sup>56</sup>
8		b		85	200–202 <sup>57</sup>
9		b		90	158–159 <sup>58</sup>
10		c		75	73–75 <sup>59</sup>
11		d		85	130–133 <sup>60</sup>
12		d		80	100–103 <sup>61</sup>
Continued					

Entry	Alcohol	Amine salt	Product	Yield (%) <sup>a</sup>	Mp. (°C) (Ref.)
13		e		87	128–130 <sup>62</sup>
14		e		85	173–175 <sup>63</sup>
15		e		90	165–166 <sup>63</sup>
16		f		93	72–74 <sup>63</sup>
17		f		87	104–106 <sup>64</sup>
18		f		94	67–69 <sup>65</sup>
19		g		75	Yellow oil <sup>63</sup>

**Table 3.** Direct oxidative amidation of benzyl alcohols with amine salts. Reaction condition: amine hydrochloride (1.0 mmol), benzyl alcohols (1.5 mmol), Catalyst (CN-Pr- $\beta$ -CD/Cu(II)) (15 mg), CH<sub>3</sub>CN (3 mL), CaCO<sub>3</sub> (1.1 equiv), TBHP (70 wt% in H<sub>2</sub>O, 3 equiv). <sup>a</sup>Isolated yield.

and dried after washing with ethanol and used again in model reaction. According to the obtained result in Fig. 8, the prepared catalyst can be reused up to 5 times in the model reaction. Catalyst leaching was also evaluated and according to the obtained results from ICP-OES, Cu% decreased from 12.7% to 12.65% after five cycles. Following the study of catalytic properties, a comparison between the synthesized catalyst and previous articles was made. Based on information summarized in the Table 4, the CN-Pr- $\beta$ -CD/Cu(II) catalyst is competitive with other reports in product efficiency, reaction time and conditions, as well as the ability to recyclability the catalyst.

### Conclusions

In this study, CN-Pr- $\beta$ -CD/Cu(II) was synthesized and evaluated as an effective catalyst for the tandem oxidative amidation of benzylic alcohols. Catalyst synthetic processes were performed via modification of CN by 1,3-dibromopropane and  $\beta$ -CD/Cu(II) respectively. CN-Pr- $\beta$ -CD/Cu(II) was evaluated and identified by using analysis such as FT-IR, XRD, FE-SEM, EDS, TGA, ICP-OES, BET, and TEM. The mentioned catalytic reaction was performed in the presence of amine hydrochloride salts, TBHP, and Ca<sub>2</sub>CO<sub>3</sub> in CH<sub>3</sub>CN solvent. The transition metal by activating the TBHP plays a key role in the progress of the reaction. According to the obtained results, the tandem oxidative amidation of benzyl alcohols with various aromatic and aliphatic amine hydrochloride salts (types I, II and III) as well as various benzyl alcohols including electron withdrawing and donor groups have been investigated. In all cases the desired amides were obtained with the appropriate yields.

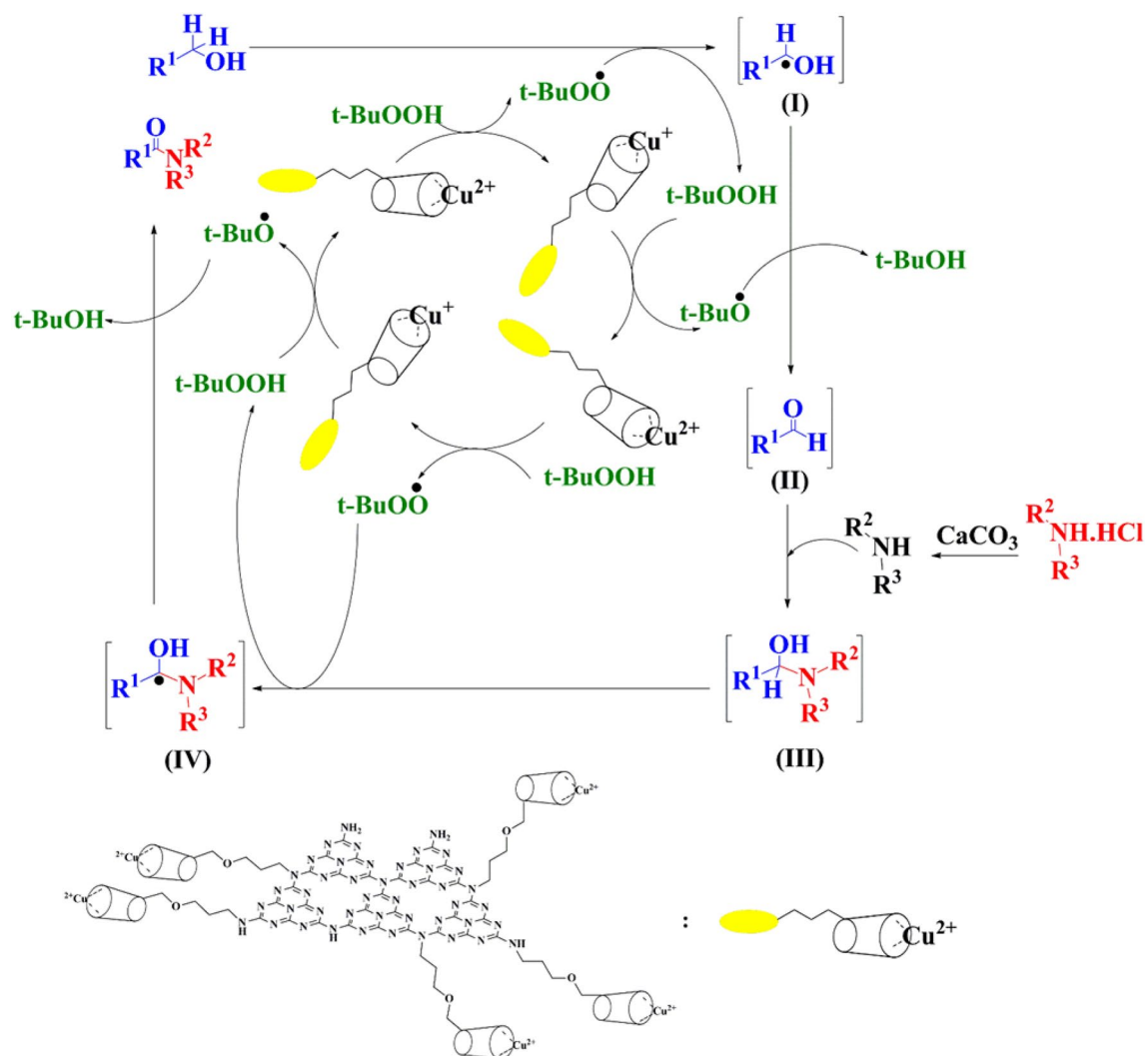


**Figure 7.** The proposed mechanism for synthesis of amide through the oxidative amidation of benzyl alcohols by CN-Pr-β-CD/Cu(II) catalyst.

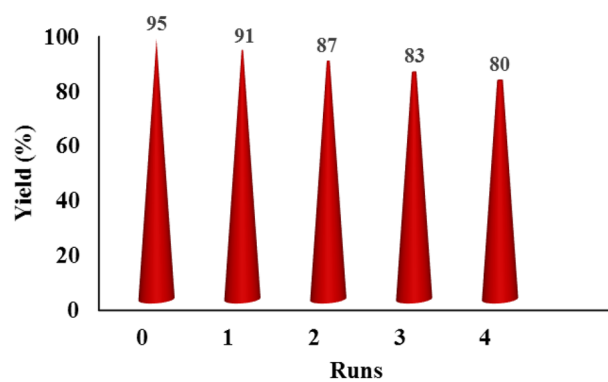


**Figure 8.** Reusability of the CN-Pr-β-CD/Cu(II) catalyst in the synthesis of amide through the oxidative amidation of benzyl alcohols.

Entry	Catalyst	Oxidizing agent	Base	Reaction time (h)	Yield (%)	References
1	Au/DNA	O <sub>2</sub>	LiOH.2H <sub>2</sub> O	12	80	69
2	Fe <sub>3</sub> O <sub>4</sub> @Fe(OH) <sub>3</sub>	TBHP	CaCO <sub>3</sub>	6	89	20
3	CuO	TBHP	CaCO <sub>3</sub>	4	70	70
4	MagCNTs@SiO <sub>2</sub> -linker-CuI	T-Hydro	Na <sub>2</sub> CO <sub>3</sub>	6	83	71
5	Au6Pd/resin	O <sub>2</sub>	NaOH	12	83	72
6	Diacetoxyiodobenzene (DIB)	TBHP	–	10	69	73
7	Fe(NO <sub>3</sub> ) <sub>3</sub>	O <sub>2</sub> /TBHP	CaCO <sub>3</sub>	16	78	74
8	(PyPS) <sub>3</sub> PW <sub>12</sub> O <sub>40</sub>	TBHP	–	12	80	75
9	CN-Pr-β-CD/Cu(II)	TBHP	CaCO <sub>3</sub>	3	95	This work

**Table 4.** Comparison between the catalytic efficiency of the CN-Pr-β-CD/Cu(II) with the reported catalysts for the amide synthesis through the oxidative amidation of benzyl alcohols.

Received: 29 September 2021; Accepted: 11 January 2022

Published online: 11 February 2022

## References

- Renuka, M. K. & Gayathri, V. A polymer supported Cu (II) catalyst for oxidative amidation of benzyl alcohol and substituted amines in TBHP/H<sub>2</sub>O. *Catal. Commun.* **104**, 71–77 (2018).
- Hollanders, K., Maes, B. U. & Ballet, S. A new wave of amide bond formations for peptide synthesis. *Synthesis* **51**, 2261–2277 (2019).
- Cui, Y., Zhang, M., Du, F. S. & Li, Z. C. Facile synthesis of H<sub>2</sub>O<sub>2</sub>-cleavable poly (ester-amide)s by passerini multicomponent polymerization. *ACS Macro Lett.* **6**, 11–15 (2017).
- Matheau-Raven, D. *et al.* Catalytic reductive functionalization of tertiary amides using Vaska's complex: Synthesis of complex tertiary amine building blocks and natural products. *ACS Catal.* **10**, 8880–8897 (2020).
- de Figueiredo, R. M., Suppo, J. S. & Campagne, J. M. Nonclassical routes for amide bond formation. *Chem. Rev.* **116**, 12029–12122 (2016).
- Pattabiraman, V. R. & Bode, J. W. Rethinking amide bond synthesis. *Nature* **480**, 471–479 (2011).
- Montalbetti, C. A. & Falque, V. Amide bond formation and peptide coupling. *Tetrahedron* **61**, 10827–10852 (2005).
- Han, S. Y. & Kim, Y. A. Recent development of peptide coupling reagents in organic synthesis. *Tetrahedron* **60**, 2447–2467 (2004).
- Liu, J. *et al.* Nitromethane as a nitrogen donor in Schmidt-type formation of amides and nitriles. *Science* **367**, 281–285 (2020).
- Chandgude, A.L., Dömling, A. N-hydroxyimide Ugi reaction toward α-hydrazino amides. *Org. Lett.* **19**, 1228–1231 (2017).
- Gololobov, Y. G. & Kasukhin, L. F. Recent advances in the Staudinger reaction. *Tetrahedron* **48**, 1353–1406 (1992).
- Jiang, D., He, T., Ma, L. & Wang, Z. Recent developments in Ritter reaction. *RSC Adv.* **4**, 64936–64946 (2014).
- Gunanathan, C., Ben-David, Y. & Milstein, D. Direct synthesis of amides from alcohols and amines with liberation of H<sub>2</sub>. *Science* **317**, 790–792 (2007).
- Allen, C. L., Atkinson, B. N. & Williams, J. M. Transamidation of primary amides with amines using hydroxylamine hydrochloride as an inorganic catalyst. *Angew. Chem. Int. Ed.* **51**, 1383–1386 (2012).
- Isaeva, V. I. & Kustov, L. M. Catalytic hydroamination of unsaturated hydrocarbons. *Top. Catal.* **59**, 1196–1206 (2016).
- Li, Z. *et al.* Palladium-catalyzed N-acylation of tertiary amines by carboxylic acids: A method for the synthesis of amides. *Org. Lett.* **22**, 5517–5521 (2020).
- Oldenhuis, N. J., Dong, V. M. & Guan, Z. Catalytic acceptorless dehydrogenations: Ru-Macho catalyzed construction of amides and imines. *Tetrahedron* **70**, 4213–4218 (2014).
- Watson, A. J., Maxwell, A. C. & Williams, J. M. Ruthenium-catalyzed oxidation of alcohols into amides. *Org. Lett.* **11**, 2667–2670 (2009).
- Wu, X. F. *et al.* The first ZnII-catalyzed oxidative amidation of benzyl alcohols with amines under solvent-free conditions. *Eur. J. Org. Chem.* **2013**, 2783–2787 (2013).
- Arefi, M., Saberi, D., Karimi, M. & Heydari, A. Superparamagnetic Fe(OH)<sub>3</sub>@Fe<sub>3</sub>O<sub>4</sub> nanoparticles: an efficient and recoverable catalyst for tandem oxidative amidation of alcohols with amine hydrochloride salts. *ACS Comb. Sci.* **17**, 341–347 (2015).
- Soulé, J. F., Miyamura, H. & Kobayashi, S. Powerful amide synthesis from alcohols and amines under aerobic conditions catalyzed by gold or gold/iron,-nickel or-cobalt nanoparticles. *J. Am. Chem. Soc.* **133**, 18550–18553 (2011).
- Owston, N. A., Parker, A. J. & Williams, J. M. Iridium-catalyzed conversion of alcohols into amides via oximes. *Org. Lett.* **9**, 73–75 (2007).
- Rashidzadeh, A., Ghafuri, H., Goodarzi, N., Azizi, N. Tandem oxidative amidation of alcohols catalyzed by copper modified well-ordered mesoporous graphitic carbon nitride. *Solid State Sci.* **109**, 106427 (2020).
- Gawande, M. B. *et al.* Cu and Cu-based nanoparticles: Synthesis and applications in catalysis. *Chem. Rev.* **116**, 3722–3811 (2016).
- Kumar, A. & Xu, Q. Two-dimensional layered materials as catalyst supports. *ChemNanoMat.* **4**, 28–40 (2018).
- Rashidzadeh, A., Ghafuri, H., Esmaili Zand, H. R. & Goodarzi, N. Graphitic carbon nitride nanosheets covalently functionalized with biocompatible vitamin B1: synthesis, characterization, and its superior performance for synthesis of quinoxalines. *ACS Omega* **4**, 12544–12554 (2019).
- Shafawi, A.N., *et al.* Bi<sub>2</sub>O<sub>3</sub> particles decorated on porous g-C<sub>3</sub>N<sub>4</sub> sheets: enhanced photocatalytic activity through a direct Z-scheme mechanism for degradation of Reactive Black 5 under UV-vis light. *J. Photochem. Photobiol. A: Chem.* **389**, 112289 (2020).
- Mohamed, M. A. *et al.* Bio-inspired hierarchical hetero-architectures of in-situ C-doped g-C<sub>3</sub>N<sub>4</sub> grafted on C, N co-doped ZnO micro-flowers with booming solar photocatalytic activity. *J. Ind. Eng. Chem.* **77**, 393–407 (2019).
- Kavil, J., Pilathottathil, S., Thayyil, M.S., Periyat, P. Development of 2D nano heterostructures based on g-C<sub>3</sub>N<sub>4</sub> and flower shaped MoS<sub>2</sub> as electrode in symmetric supercapacitor device. *Nano-Struct. Nano-Objects.* **18**, 100317 (2019).
- Mishra, A. *et al.* Graphitic carbon nitride (g-C<sub>3</sub>N<sub>4</sub>)-based metal-free photocatalysts for water splitting: A review. *Carbon* **149**, 693–721 (2019).
- Lee, S. P., Lee, J. G. & Chowdhury, S. CMOS humidity sensor system using carbon nitride film as sensing materials. *Sensors* **8**, 2662–2672 (2008).
- Zou, X., Silva, R., Goswami, A. & Asefa, T. Cu-doped carbon nitride: Bio-inspired synthesis of H<sub>2</sub>-evolving electrocatalysts using graphitic carbon nitride (g-C<sub>3</sub>N<sub>4</sub>) as a host material. *Appl. Surf. Sci.* **357**, 221–228 (2015).

33. Moussa, H. *et al.* Growth of ZnO nanorods on graphitic carbon nitride gCN sheets for the preparation of photocatalysts with high visible-light activity. *ChemCatChem* **10**, 4973–4983 (2018).
34. Kairouz, V. & Schmitzer, A. R. Imidazolium-functionalized  $\beta$ -cyclodextrin as a highly recyclable multifunctional ligand in water. *Green Chem.* **16**, 3117–3124 (2014).
35. Matencio, A., Navarro-Orcajada, S., García-Carmona, F. & López-Nicolás, J. M. Applications of cyclodextrins in food science A review. *Trends Food Sci. Technol.* **104**, 132–143 (2020).
36. Braga, S. S. Cyclodextrins: emerging medicines of the new millennium. *Biomolecules* **9**, 801 (2019).
37. Singh, N. & Sahu, O. The impact and prospects of green chemistry for textile technology. *Elsevier* **1**, 83–105 (2019).
38. Rabaça, M.S., Dermatological and cosmetic applications of cyclodextrins. Doctoral dissertation, Universidade de Coimbra (2019).
39. Sonnendecker, C. *et al.* Large-ring cyclodextrins as chiral selectors for enantiomeric pharmaceuticals. *Angew. Chem.* **131**, 6477–6480 (2019).
40. Zou, Y. *et al.*  $\beta$ -Cyclodextrin modified graphitic carbon nitride for the removal of pollutants from aqueous solution: experimental and theoretical calculation study. *J. Mater. Chem. A* **4**, 14170–14179 (2016).
41. Zhen, X. V. *et al.* Noncovalent monolayer modification of graphene using pyrene and cyclodextrin receptors for chemical sensing. *ACS Appl. Nano Mater.* **1**, 2718–2726 (2018).
42. Bai, C. C., Tian, B. R., Zhao, T., Huang, Q. & Wang, Z. Z. Cyclodextrin-catalyzed organic synthesis: Reactions, mechanisms, and applications. *Molecules* **22**, 1475 (2017).
43. Zuo, G. *et al.* A  $\beta$ -cyclodextrin modified graphitic carbon nitride with Au Co-catalyst for efficient photocatalytic hydrogen peroxide production. *Nanomaterials* **10**, 1969 (2020).
44. Zhu, H. *et al.* Decorating Pt@ cyclodextrin nanoclusters on  $C_3N_4$ /MXene for boosting the photocatalytic  $H_2O_2$  production. *J. Mater. Chem.* **9**, 6872–6880 (2021).
45. Zheng, Y., Lin, L., Ye, X., Guo, F. & Wang, X. Helical graphitic carbon nitrides with photocatalytic and optical activities. *Angew. Chem.* **126**, 12120–12124 (2014).
46. Li, C. Z. *et al.* Graphitic carbon nitride nanosheet coated carbon black as a high-performance PtRu catalyst support material for methanol electrooxidation. *J. Mater. Chem. A* **2**, 20139–20146 (2014).
47. Kaboudin, B., Abedi, Y. & Yokomatsu, T. One-pot synthesis of 1, 2, 3-triazoles from boronic acids in water using Cu (II)- $\beta$ -cyclodextrin complex as a nanocatalyst. *Org. Biomol. Chem.* **10**, 4543–4548 (2012).
48. Fina, F., Callear, S. K., Carins, G. M. & Irvine, J. T. Structural investigation of graphitic carbon nitride via XRD and neutron diffraction. *Chem. Mater.* **27**, 2612–2618 (2015).
49. Lin, B. *et al.* Fish-scale structured g- $C_3N_4$  nanosheet with unusual spatial electron transfer property for high-efficiency photocatalytic hydrogen evolution. *Appl. Catal. B: Environ.* **210**, 173–183 (2017).
50. Kajihara, K., Arisawa, M. & Shuto, S. A method for cleaving an allyl protecting group at the amide nitrogen of peptides by one-pot olefin isomerization–oxidation. *J. Org. Chem.* **73**, 9494–9496 (2008).
51. Bian, Y. J., Chen, C. Y. & Huang, Z. Z. Synthesis of imides by palladium-catalyzed C-H functionalization of aldehydes with secondary amides. *Chem. Eur. J.* **19**, 1129–1133 (2013).
52. Howard, E. L., Guzzardi, N., Tsanova, V. G., Stika, A. & Patel, B. Highly efficient copper-catalyzed amidation of benzylic hydrocarbons under neutral conditions. *Eur. J. Org. Chem.* **2018**, 794–497 (2018).
53. Li, F., Ma, J., Lu, L., Bao, X. & Tang, W. Combination of gold and iridium catalysts for the synthesis of N-alkylated amides from nitriles and alcohols. *Catal. Sci. Technol.* **5**, 1953–1960 (2015).
54. Kawagoe, Y., Moriyama, K. & Togo, H. Facile preparation of amides from carboxylic acids and amines with ion-supported  $Ph_3P$ . *Tetrahedron* **69**, 3971–3977 (2013).
55. Teter, D. M. & Hemley, R. J. Low-compressibility carbon nitrides. *Science* **271**, 53–55 (1996).
56. Mao, J. *et al.* Effect of graphitic carbon nitride microstructures on the activity and selectivity of photocatalytic  $CO_2$  reduction under visible light. *Catal. Sci. Technol.* **3**, 1253–1260 (2013).
57. Sharma, R., Vishwakarma, R. A. & Bharate, S. B. Ligand-free copper-manganese spinel oxide-catalyzed tandem one-pot C-H amidation and N-arylation of benzylamines: A facile access to 2-arylquinazolin-4 (3H)-ones. *Adv. Synth. Catal.* **358**, 3027–3033 (2016).
58. Mukhopadhyay, S., Yaghmur, A., Benichou, A. & Sasson, Y. Homogeneous  $RuCl_2(PPh_3)_3$ -catalyzed regioselective liquid-phase transfer hydrogenation of carbon–carbon double bond in chlorobenzylidene ketones with ethylene glycol as hydrogen donor. *Org. Process Res. Dev.* **4**, 571–574 (2000).
59. Bäckvall, J. E. Transition metal hydrides as active intermediates in hydrogen transfer reactions. *J. Organomet. Chem.* **652**, 105–111 (2002).
60. Sharma, P. & Sasson, Y. A photoactive catalyst  $Ru-gC_3N_4$  for hydrogen transfer reaction of aldehydes and ketones. *Green Chem.* **19**, 844–852 (2017).
61. Huang, S., Zhao, Y. & Tang, R. Facile fabrication of a  $Cu@gC_3N_4$  nanocatalyst and its application for the aerobic oxidations of alkylaromatics and the reduction of 4-nitrophenol. *RSC Adv.* **6**, 90887–90896 (2016).
62. Sun, C., Qu, P. & Li, F. Rearrangement of aldoximes to amides in water under air atmosphere catalyzed by water-soluble iridium complex  $[Cp^*Ir(H_2O)_3][OTf]_2$ . *Catal. Sci. Technol.* **4**, 988–996 (2014).
63. Karimi, M., Ghandi, L., Saberi, D. & Heydari, A. Copper-amino group complexes supported on silica-coated magnetite nanoparticles: Efficient catalyst for oxidative amidation of methyl arenes. *New J. Chem.* **42**, 3900–3908 (2018).
64. Mei, C., Hu, Y. & Lu, W. Visible-light-driven oxidation of n-alkylamides to imides using oxone/ $H_2O$  and catalytic KBr. *Synthesis* **50**, 2999–3005 (2018).
65. Wu, Y. *et al.* Mesoporous graphitic carbon nitride and carbon– $TiO_2$  hybrid composite photocatalysts with enhanced photocatalytic activity under visible light irradiation. *J. Environ. Chem. Eng.* **4**, 797–807 (2016).
66. Punniyamurthy, T. & Rout, L. Recent advances in copper-catalyzed oxidation of organic compounds. *Coord. Chem. Rev.* **252**, 134–154 (2008).
67. Rothenberg, G., Feldberg, L., Wiener, H., Sasson, Y. Copper-catalyzed homolytic and heterolytic benzylic and allylic oxidation using tert-butyl hydroperoxide. *J. Chem. Soc., Perkin Trans. 2.* **11**, 2429–2434 (1998).
68. Tan, B., Toda, N. & Barbas, C. F. Organocatalytic amidation and esterification of aldehydes with activating reagents by a cross-coupling strategy. *Angew. Chem. Int. Ed.* **51**, 12538–12541 (2012).
69. Wang, Y., Zhu, D., Tang, L., Wang, S. & Wang, Z. Highly efficient amide synthesis from alcohols and amines by virtue of a water-soluble gold/DNA catalyst. *Angew. Chem. Int. Ed.* **50**, 8917–8921 (2011).
70. Bantreil, X., Fleith, C., Martinez, J. & Lamaty, F. Copper-catalyzed direct synthesis of benzamides from alcohols and amines. *ChemCatChem* **4**, 1922–1925 (2012).
71. Saberi, D. & Heydari, A. Oxidative amidation of aromatic aldehydes with amine hydrochloride salts catalyzed by silica-coated magnetic carbon nanotubes (MagCNTs@ $SiO_2$ )-immobilized imine–Cu (I). *Appl. Organomet. Chem.* **28**, 101–108 (2014).
72. Zhang, L. *et al.* Aerobic oxidative coupling of alcohols and amines over Au–Pd/resin in water: Au/Pd molar ratios switch the reaction pathways to amides or imines. *Green Chem.* **15**, 2680–2684 (2013).
73. Sutar, Y. B., Bhagat, S. B. & Telvekar, V. N. General and efficient oxidative amidation of benzyl alcohols with amines using diacetoxyiodobenzene and TBHP. *Tetrahedron Lett.* **56**, 6768–6771 (2015).

74. Ghosh, S. C. *et al.* Tandem oxidative amidation of benzyl alcohols with amine hydrochloride salts catalysed by iron nitrate. *Tetrahedron Lett.* **54**, 4922–4925 (2013).
75. Fu, R. *et al.* An efficient, eco-friendly and sustainable tandem oxidative amidation of alcohols with amines catalyzed by heteropolyanion-based ionic liquids via a bifunctional catalysis process. *Tetrahedron* **72**, 8319–8326 (2016).

### Acknowledgements

The authors gratefully acknowledge the partial support from the Research Council of the Iran University of Science and Technology.

### Author contributions

H.G.: the corresponding (submitting) author of current study, substantial contributions to the conception, design of the work, have drafted the work, writing—review and editing, substantively revised it. A.R.: substantial contributions to the conception, design of the work, analysis and interpretation of data and wrote the main manuscript. M.G.G.: have drafted the work, analysis and interpretation of data, substantively revised it. Wrote the main manuscript and prepared figures. G.J.: analysis and interpretation of data.

### Competing interests

The authors declare no competing interests.

### Additional information

**Correspondence** and requests for materials should be addressed to H.G.

**Reprints and permissions information** is available at [www.nature.com/reprints](http://www.nature.com/reprints).

**Publisher's note** Springer Nature remains neutral with regard to jurisdictional claims in published maps and institutional affiliations.



**Open Access** This article is licensed under a Creative Commons Attribution 4.0 International License, which permits use, sharing, adaptation, distribution and reproduction in any medium or format, as long as you give appropriate credit to the original author(s) and the source, provide a link to the Creative Commons licence, and indicate if changes were made. The images or other third party material in this article are included in the article's Creative Commons licence, unless indicated otherwise in a credit line to the material. If material is not included in the article's Creative Commons licence and your intended use is not permitted by statutory regulation or exceeds the permitted use, you will need to obtain permission directly from the copyright holder. To view a copy of this licence, visit <http://creativecommons.org/licenses/by/4.0/>.

© The Author(s) 2022